Dedicated to Professor Dr. rer. nat. Dr.-Ing. E. h. Hans-Jürgen Engell in honour of his 65th birthday

Modelling of crystal growth during the ribbon formation in planar flow casting

Andreas Ludwig, Georg Frommeyer and László Gránásy

The crystalline solidification during rapid substrate quenching in planar-flow casting was simulated by using a numerical model based on a rapid solidification algorithm and the infinite viscosity approximation. The calculation shows that the existence of a real melt puddle shape suppresses undercooling and recalescence on the melt surface as well as on the solidifying ribbon. The melt puddle length is mainly determined by the heat-transfer coefficient. With increasing heat transfer across the melt – substrate interface the melt puddle length decreases.
If the formation rate of critical nuclei on the substrate surface is low compared to the present cooling rate a large undercooling may occur. The performed calculations reveal that an undercooling of up to 600 K does neither affect the temperature distribution on the surface of the melt nor the melt puddle length, perceptibly. Therefore, investigations on microstructural features of rapidly quenched metals might give detailed information on the amount of undercooling present at the beginning of solidification.

Modellierung der kristallinen Erstarrung während der Bandentstehung beim Planar Flow Casting. Es wurde die kristalline Erstarrung bei der Bandentstehung während des Planar Flow Casting-Prozesses simuliert, wobei ein numerisches Modell benutzt wurde, daß auf einem Algorithmus für die rasche Erstarrung sowie der „infinite viscosity approximation" beruht. Die Berechnungen zeigen, daß die Existenz eines Schmelzsumpfes das Auftreten von Unterkühlung und Rekaleszenz auf der Oberseite des erstarrenden Bandes unterdrückt. Die Länge des Schmelzsumpfes ist im wesentlichen durch den Wärmeübergangskoeffizienten gegeben. Je größer der Wärmefluß durch die Grenzfläche Schmelze – Substrat ist, desto kürzer ist der sich ausbildende Schmelzsumpf.
Ist die Keimbildungsrate an der Substratoberfläche niedrig, verglichen mit der auftretenden Abkühlrate, so können hohe Unterkühlungen auftreten. Die durchgeführten Berechnungen zeigen, daß Unterkühlungen bis zu 600 K weder die Temperaturverteilung auf der Schmelzenoberfläche noch die Schmelzsumpflänge nennenswert beeinflussen. Über die beim Erstarrungsbeginn auftretenden Unterkühlungen können Untersuchungen des Mikrogefüges der Bänder detailierte Information geben.

Materials with metastable microstructures and superior properties produced by rapid solidification have been studied in the last few years[1)2)] and continue to be the subject of intensive research activities. Especially melt spinning by planar-flow casting (PFC) used for the continuous production of ribbons is of great technological importance. An interesting aspect in this field is the relation between the heat-flow characteristics, the solidification behaviour and the resultant microstructure.

Considering the solidification of highly undercooled and levitated melts, the structural features of melt-spun ribbons can be understood when a high undercooling in the melt puddle–substrate contact regime occurs[3)]. An evidence supporting this view might be the fact that amorphous material can easily be produced by melt spinning[1)].

In contrast to this no recalescence phenomena caused by high undercooling of crystalline solidifying materials have been detected on the top of the melt puddle by pyrometry or colour photometry[4)5)].

The present paper discusses the influence of the heat-transfer coefficient, the undercooling and the melt puddle shape on the temperature distribution within the liquid – solid region during the formation of crystalline ribbons produced by planar-flow casting. The results are based on a numerical model for rapid substrate quenching.

Information from the Max-Planck-Institut für Eisenforschung GmbH, Düsseldorf, paper 1551.
Dipl.-Phys. Andreas Ludwig; Professor Dr.-Ing. Georg Frommeyer, Abt. Werkstofftechnik, Max-Planck-Institut für Eisenforschung GmbH, Düsseldorf, FRG; *Dr. rer. nat. László Gránásy*, Central Research Institute for Physics, Budapest, Hungary.

Description of the numerical model

In order to model the formation of crystalline ribbons by planar-flow casting the heat as well as the mass transfer, the a priori unknown free surface of the melt puddle, and the heat release at the solid–liquid interface have to be taken into account. The latter is given by the process conditions. A schematic drawing of the melt puddle – substrate arrangement is shown in **figure 1**.

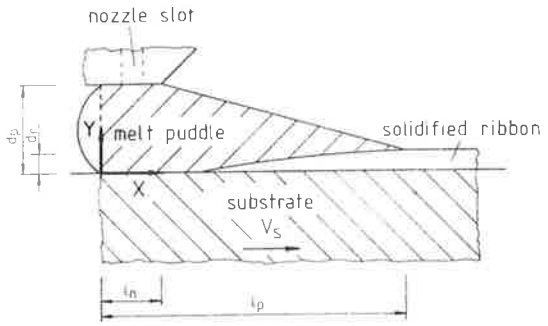

Figure 1. Typical melt puddle shape of planar-flow casting
d_p: gap between nozzle and substrate
d_r: thickness of the ribbon
l_p: melt puddle length
l_n: nozzle melt contact length

Bild 1. Typische Schmelzsumpfform des Planar Flow Casting
d_p: Abstand zwischen Düse und Rad
d_r: Banddicke
l_p: Schmelzsumpflänge
l_n: Länge des Kontaktes zwischen Düse und Schmelze

For a proper treatment of this problem the following assumptions have been established:
- the flow field is constant and the field vector is identical with the tangential wheel velocity $\vec{v}_s$;
- the heat flow in x-direction (figure 1) is mainly caused by the thermal convection, so the conductive term in x-direction will be neglected;
- the surface of the melt puddle is approximately represented as a straight line (figure 1).

The assumption of a constant flow field is known as the infinite viscosity approximation. It has been shown that the temperature distribution within the melt puddle is not much affected by the deviation from the real flow field[6]).

The heat transfer is described quantitatively by a one-dimensional differential equation using a heat-source term $\dot{Q}$ for the release of the latent heat of fusion as:

$$\frac{dT}{dt} = \frac{k}{\rho c_p} \cdot \frac{d^2T}{dy^2} + \frac{\dot{Q}}{\rho c_p}, \tag{1}$$

where k is the thermal conductivity, ρ is the density and c_p determines the specific heat capacity. This equation has been approximated by using a central difference scheme for the spatial derivation, and a forward difference scheme for the time derivation.

Starting from the current temperature of the elements i, $i-1$ and $i+1$ at a time t, the new temperature of the element i at the time $t + \Delta t$ is obtained by the difference equation:

$$T_i^n = T_i + \frac{k}{\rho c_p} \cdot \frac{\Delta t}{\Delta y^2} (T_{i+1} + T_{i-1} - 2T_i) + \frac{\dot{Q}_i}{\rho c_p}. \tag{2}$$

A typical spatial element $\Delta y = 2.5$ µm has been used. According to T. W. Clyne[7]) this spatial element would limit the accompanying time step Δt, if a stable solution of equation (2) will be achieved.

For planar-flow casting normally a nozzle substrate gap of about 500 µm is used to produce ribbons with 100 µm in thickness or less, respectively. A stable melt puddle with a nearly round shape of the leading edge is formed. High-speed recordings show that the melt puddle developed is of the order of several centimeters in length. This depends on the properties of the chosen materials (e.g. the viscosity of the melt, the heat conductivity of the wheel etc.), the wheel velocity, and the ribbon thickness.

Due to the constant flow field condition, the time step Δt can be expressed as a spatial element $\Delta x = v_s \cdot \Delta t$. Starting with $t = 0$ and going to $t = t_{end}$ implies that the calculation ranges from $x = 0$ to $x = x_{end}$.

Boundary conditions. The calculations of the temperature distribution were performed for the melt puddle as well as for the mantel zone of the rotating wheel. The upper edge of the melt puddle including the orifice of the crucible, as well as the left and the lower edge of the hatched area was set at the initial melt temperature T_M and the initial wheel temperature T_w, respectively.

Cooling of the free surface of both the melt and the ribbon is neglected. For the melt-wheel contact zone a large heat-transfer coefficient h in the order of $>10^5$ W/m^{2}K was considered. The heat flow Q_{tr} across the interface is given by the expression:

Table 1. List of symbols

Tafel 1. Erläuterung der Formelzeichen

ΔH_f	enthalpy of fusion (17,13 kJ/mol)
T_f	melting point of Ni (1 728 K)
ρ	density of Ni (8 910 kJ/m^3)
c_p	heat capacity of Ni (594 J/kg K)
k_c	heat conductivity of liquid Ni at T_f (30 W/m K)
k_s	heat conductivity of solid Ni at T_f (88.5 W/m K)
λ	diffusion jump distance (0,23 nm)
η_0	defined by the Vogel-Fulcher expression for η ($1663 \cdot 10^{-4}$ Pa · s)
B_0	defined by the Vogel-Fulcher expression for η (6 035.8 K)
T_0	defined by the Vogel-Fulcher expression for η (0 K)
ρ_w	density of Cu (8 920 kg/m^3)
c_{pw}	heat capacity of Cu (380 J/kg K)
k_w	heat conductivity of Cu at room temperature (401 W/m K)

$$Q_{tr} = h(T_{melt} - T_{wheel}), \tag{3}$$

where T_{melt} defines the melt temperature, and T_{wheel} is the wheel temperature in the melt – wheel contact area.

The release of the latent heat of fusion. Crystal growth starts at the bottom of the melt puddle when a definite undercooling of the liquid is reached. The mushy zone, accompanying the moving solid–liquid interface, was assumed to be smaller than the cell spacing ($\Delta y \sim 2.5$ µm).

In the time step Δt the interface moves the distance $U \cdot \Delta t$. The volume fraction f of the element containing the solid–liquid interface changes after Δt to $f + \Delta f = f + U\,\Delta t/\Delta x$. The heat release associated with this advance results in a source term as:

$$\dot{Q} = \frac{\Delta f}{\Delta t} \cdot \Delta H_f = \frac{U(\Delta T)}{\Delta x} \cdot \Delta H_f, \tag{4}$$

where ΔH_f is the heat of fusion. This source term is added to the volume elements which are adjacent to the interface. Therefore, the release of the latent heat leads to a heating up of an attached zone of Δy in width.

Growth kinetics. The classical treatment of continuous crystal growth leads to the following expression for the growth rate:

$$U(T) = \frac{D_L}{\lambda}\left[1 - \exp\left(-\frac{\Delta H_f \cdot \Delta T}{T_f \cdot k_B T}\right)\right], \tag{5}$$

where T_f defines the melting temperature, ΔT is the undercooling of the interface, λ is the diffuse jump distance, and D_L is the liquid diffusion coefficient.

The liquid diffusion coefficient D_L is derived from the Einstein-Stokes relation and the Vogel-Fulcher expression for the viscosity η:

$$D_L(T) = \frac{k_B T}{3\pi\lambda\eta(T)} = \frac{k_B T}{3\pi\lambda\eta_0}\exp\left(\frac{-B_0}{T - T_0}\right). \tag{6}$$

All calculations were performed for a Ni melt on a Cu wheel. The thermophysical data used are given in **table 1.**

Results and discussion

The effect of undercooling on solidification. In rapid substrate quenching the amount of undercooling arising during the formation of critical nuclei with subsequent solidification is still an open question. Assuming convention-

al solidification behaviour, one starts from an epitaxial growth where nucleation is not necessary because the crystals start to grow on the substrate immediately when the melt cools below the solidification temperature. In rapid substrate quenching epitaxial growth is only possible when the liquid and the substrate are of the same material and no oxide layer is formed on the substrate surface. On the other hand, the solidification of a melt to amorphous ribbons indicates that undercoolings of several hundred degrees may occur. For example, the melting temperature T_f and the temperature of the glass transition T_g for $Fe_{83}B_{17}$ are 1448 and 700 K[8]), respectively. Therefore an undercooling of about 748 K for the glass formation of $Fe_{83}B_{17}$ is necessary.

In order to study the influence of undercooling on the formation of a 50 µm thick Ni ribbon on a Cu wheel, the initial wheel temperature was defined with 25 °C and the constant wheel velocity was chosen with 10 m/s. The initial melt temperature was set at 1828 K, considering a superheating of 100 K.

The distance between the wheel surface and the nozzle was set at 500 µm, therefore, the height of the melt puddle is ten times larger than the thickness of the as-solidified ribbon. The nozzle melt contact length was defined with 2 mm.

The melt puddle length was iteratively calculated so that the end of the melt puddle and the point where the solidification of the ribbon is completed, coincide. This procedure is based on the theory of the thermally controlled ribbon formation, which seems to be realistic for large heat-transfer coefficients ($h > 10^5$ W/m^{2}K)[4]).

Modelling was carried out for different nucleation time intervals, using a constant heat-transfer coefficient of $5 \cdot 10^5$ W/m^{2}K. The crystal growth starts when the melt temperature reaches the given undercooling. The resulting temperature distributions within a melt puddle are shown in **figure 2.**

The ribbon surface temperature which can be experimentally determined by fast infrared pyrometric measurements[9]) or thermovision techniques[10])[11]) is shown in **figure 3.**

For epitaxial growth ($\Delta T = 0$ K) the temperature distribution within the melt puddle is very similar to that of figure 2a ($\Delta T = 300$ K). The only difference is that the solidification starts right at the leading edge of the melt puddle and a "cold spot" at the beginning of the solidification does not occur. Figure 3 indicates, that for undercoolings up to 600 K the temperature distribution on the surface of the puddle is not so much affected by the undercooling and the length of the puddle is nearly constant.

Contrary to this a large undercooling of 900 K (figure 2c) leads to a significally different characteristic of the surface temperature distribution. Recalescence and a considerable melt-puddle extension by a factor of five will be expected.

This behaviour may be explained by the thermal transport within the substrate. During the cooling process the substrate temperature increases and the melt temperature decreases, so the temperature gap at the substrate–melt interface diminishes. This results in a decrease of the average cooling rate. For $\Delta T = 300$ K a cooling rate of $5 \cdot 10^6$ K/s and for $\Delta T = 600$ K a value of $2 \cdot 10^6$ K/s has been estimated. For an extremely large undercooling of 900 K the cooling rate decreased to $3 \cdot 10^5$ K/s.

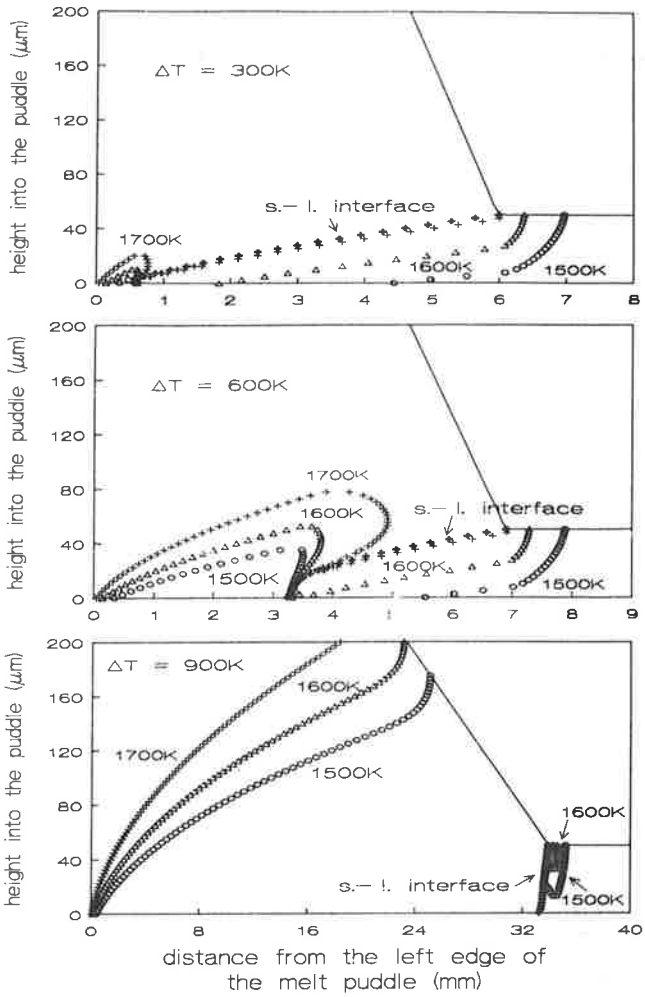

Figure 2. Temperature distribution within the melt puddle for three different undercoolings
a) $\Delta T = 300$ K, b) $\Delta T = 600$ K, c) $\Delta T = 900$ K (heat-transfer coefficient $h = 5 \cdot 10^5$ W/m^{2}K)

Bild 2. Temperaturverteilung innerhalb des Schmelzsumpfes für drei unterschiedliche Unterkühlungen
a) $\Delta T = 300$ K, b) $\Delta T = 600$ K, c) $\Delta T = 900$ K (Wärmeübergangskoeffizient $h = 5 \cdot 10^5$ W/m^{2}K)

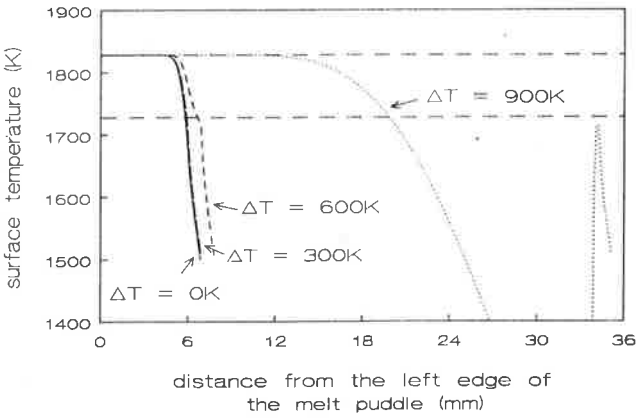

Figure 3. Surface temperature of the melt puddle for different undercoolings (heat-transfer coefficient $h = 5 \cdot 10^5$ W/m^{2}K)

Bild 3. Oberflächentemperatur des Schmelzsumpfes für unterschiedliche Unterkühlungen (Wärmeübergangskoeffizient $h = 5 \cdot 10^5$ W/m^{2}K)

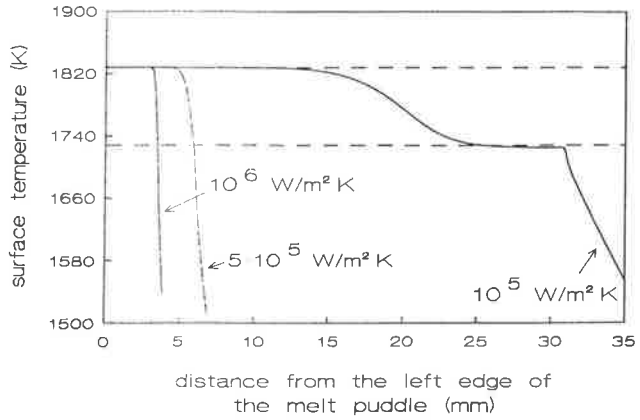

Figure 4. Surface temperature of the melt puddle for three different heat-transfer coefficients

Bild 4. Oberflächentemperatur des Schmelzsumpfes für drei verschiedene Wärmeübergangskoeffizienten

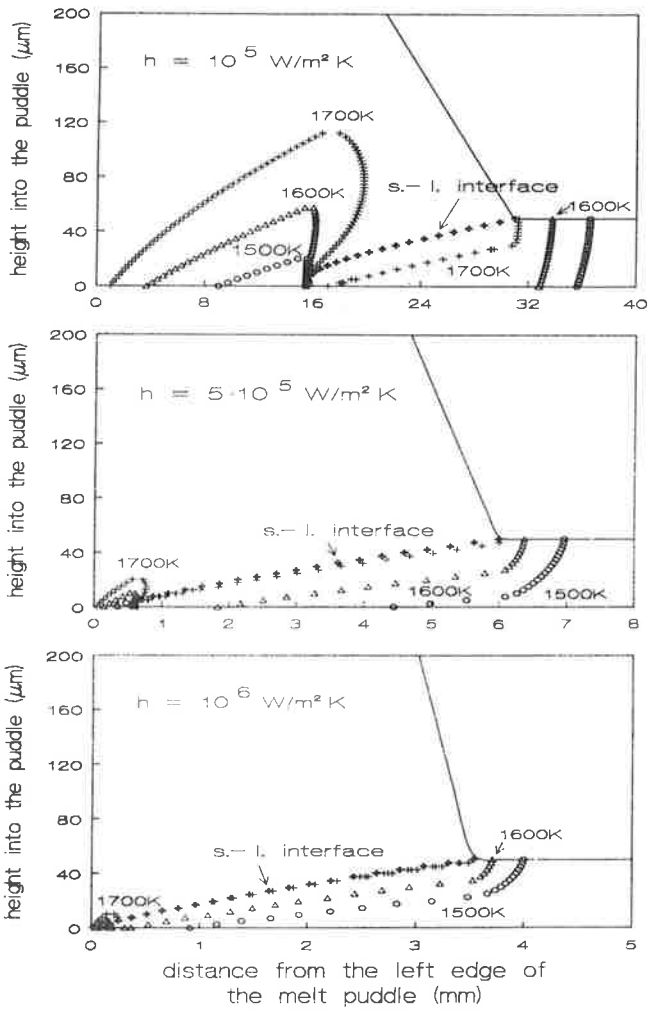

Figure 5. Temperature distribution within the melt puddle for three different heat-transfer coefficients
a) $h = 10^5$ W/m²K, b) $h = 5 \cdot 10^5$ W/m²K, c) $h = 10^6$ W/m²K (undercooling $\Delta T = 300$ K)

Bild 5. Temperaturverteilung innerhalb des Schmelzsumpfes für drei verschiedene Wärmeübergangskoeffizienten
a) $h = 10^5$ W/m²K, b) $h = 5 \cdot 10^5$ W/m²K, c) $h = 10^6$ W/m²K (Unterkühlungstemperatur $\Delta T = 300$ K)

The different cooling rates result in an exponential relationship between the amount of undercooling and the related time interval.

Generally, the crystalline solidification in rapid substrate quenching can be devided into two stages. In the first stage the crystal growth is determined by the undercooling present at the melt–substrate interface and the accompanying high growth rate. This results in a relatively steep slope of the curvatures of the liquid–solid interfaces in figures 2a–c. With increasing melt temperatures at the interface, due to the release of latent heat of fusion, the growth rate decreases until the rate of heat release and the rate of heat dissipation is balanced. In this stage the growth is controlled by the heat flux. The related undercooling is of the order of 1–20 K and, therefore, the growth rate is relatively low. This results in the flat regimes of the solid-liquid interface (figures 2a and b).

At medium undercooling of 300 K the solidification is mainly heat-flux controlled and at the extremely high undercooling of 900 K the solidification is completely controlled by the high undercooling. For $\Delta T = 600$ K the solidification is partly controlled by the undercooling and by the heat flux.

The influence of the heat transfer coefficient on the solidification. In order to perform a comparative analysis, computations were carried out by varying the heat-transfer coefficient from 10^5 to 10^6 W/m²K. These simulations are based on the same parameters as described in the last section, taking an undercooling of 300 K into account.

The melt-pool surface temperature is depicted in **figure 4** and the temperature distribution within the melt puddle is illustrated in **figure 5.** Figures 5a–c shows that the length of the melt puddle is correlated with the heat-transfer coefficient. A large heat-transfer coefficient results in a short melt puddle. This is principally caused by two facts. With an increasing heat-transfer coefficient the average cooling rate at the melt–substrate interface increases, therefore, the actual undercooling is reached sooner than with a small heat-transfer coefficient. If the heat-transfer coefficient is equal to 10^5 W/m²K an average cooling rate of $2 \cdot 10^5$ K/s occurs and for the maximum heat-transfer coefficient of 10^6 W/m²K an extremly high cooling rate of $1.5 \cdot 10^7$ K/s will be expected.

Considering large heat-transfer coefficients the undercooling in the heat-flux controlled region is increased, because of the preferential heat transport. This results in a higher solidification rate and, thus, a steeper slope of the solid–liquid interface will be formed. Consequently, the zone which is controlled by the undercooling shrinks with increasing heat-transfer coefficient.

In addition to this a reduced heat transfer across the interface and an accompanying enlargement of the melt puddle leads to a recalescence effect on the puddle surface (figure 4).

The influence of the melt puddle shape on the temperature distribution. The influence of a real melt puddle shape on the surface temperature and the temperature distribution within the puddle as well as in the solidified ribbon is illustrated in **figures 6 and 7.** For the real melt puddle shape the surface temperature is constant up to 5 mm from the left melt puddle edge. Then the temperature decreases monotonously with increasing distance. In contrast to this the

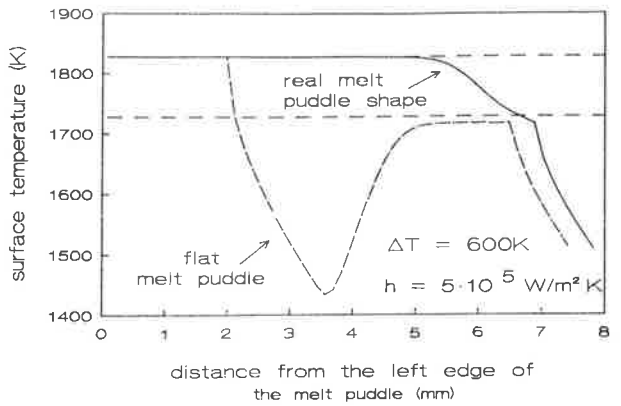

Figure 6. Surface temperature curves of a real and a flat melt puddle for $h = 5 \cdot 10^5$ W/m^{2}K and $\Delta T = 600$ K

Bild 6. Verlauf der Oberflächentemperaturen eines realen und eines flachen Schmelzsumpfes für $h = 5 \cdot 10^5$ W/m^2/K und $\Delta T = 600$ K

surface of the flat melt puddle cools down more rapidly, due to the restricted melt puddle height. Correspondingly, a marked undercooling followed by recalescence will occur.

A comparison of the temperature distributions within the melt puddle (figures 7a/b) reveals that the isotherms in the liquid of a real melt puddle are closed. Whereas the shape of the solid – liquid interface as well as the isotherms in the solidified region are not affected by the melt puddle shape.

Conclusion

Numerical model calculations based on a rapid solidification algorithm and an infinite viscosity approximation were performed for the simulation of the temperature distribution on the free surfaces, in the melt puddle and in the solidified ribbon in PFC melt spinning.

If the formation of the critical nuclei takes place within the time period in which the change of the cooling rate at the melt – substrate interface is negligible, the amount of undercooling does not affect the melt puddle size or the puddle surface temperature remarkably.

During the solidification of Ni ribbons on a Cu wheel the surface temperature of the melt puddle is not affected when the undercooling is lower than about 600 K and the heat-transfer coefficient is of the order of $5 \cdot 10^5$ W/m^{2}K.

The surface temperature and the length of the melt-puddle are determined by the heat-transfer coefficient. With increasing heat-transfer coefficient the length of the melt puddle decreases.

If the melt puddle height is reduced to an anomalous flat one, the undercooling at the beginning of the solidification governs the temperature distribution on the ribbon surface.

The solidification of the ribbon takes place in two stages: at the beginning the crystal growth is controlled by the amount of the current undercooling. Therefore, high growth rates can occur.

After the growth rate has been decreased to a certain value determined by the heat-transfer coefficient the solidification becomes heat-transport controlled while the growth rate is relatively low.

Recalescence and undercooling phenomena on the melt

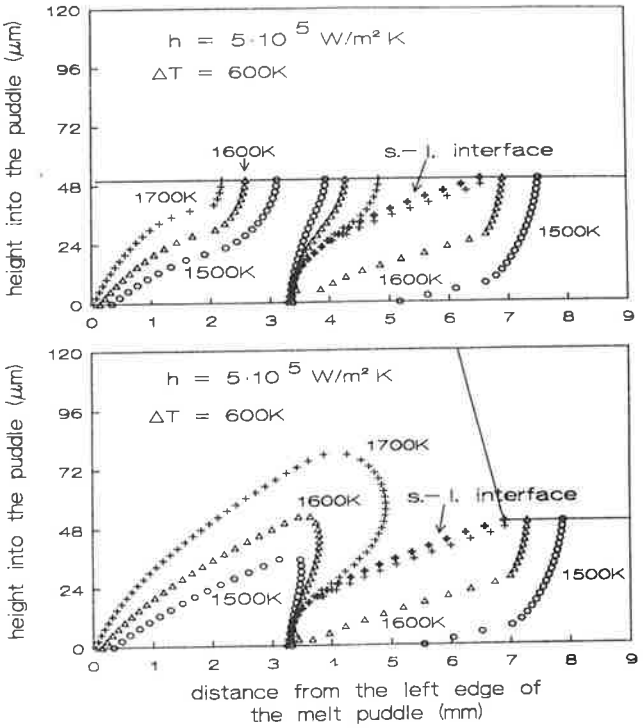

Figure 7. Temperature distribution within a flat (a) and a real (b) melt puddle for $h = 5 \cdot 10^5$ W/m^{2}K and $\Delta T = 600$ K

Bild 7. Temperaturverteilung innerhalb eines flachen (a) und eines realen Schmelzsumpfes (b) für $h = 5 \cdot 10^5$ W/m^{2}K und $\Delta T = 600$ K

puddle surface occur when the undercooling is extremely high and the heat-transfer coefficient is low. In addition to this, the melt puddle height should be kept as small as possible. In order to study undercooling and crystal growth of rapidly solidified melt-spun ribbons produced by planar-flow casting it is necessary to consider microstructural features such as grain inclination, textures and the appearance of special morphologies, e.g. cellular – dendritic transition zones or partitionless solidified areas.

Acknowledgements

The authors gratefully acknowledge the financial support of the Deutsche Forschungsgemeinschaft under Contract No. Fr. 543/7. (A 00 480; received: 23. June 1990)

References

1) *Jones, H.:* "Rapid Solidification of Metals and Alloys", Institution of Metallurgists, London, 1982.
2) *Heinemann, W. A.:* Proc. 5th Int. Conf. on Rapidly Quenched Metals, [eds.:] S. Steeb, H. Warlimont, Elsevier (1985), p. 27–34.
3) *Caesar, C.; Köster, U.; Willnecker, R.; Herlach, D. M.:* Mat. Sci. Eng. 98 (1988), p. 339–42.
4) *Vogt, E.:* Int. J. of Rapid Sol. 3 (1987), p. 131–46.
5) *Gillen, A. G.; Cantor, B.:* Acta Met. 33 (1985), p. 1813–25.
6) *Gránásy, L.; Mészáros, G.:* Mat. Sci. Eng. 72 (1985), p. 71–83.
7) *Clyne, T. W.:* Met. Trans. 15B (1984), p. 369–81.
8) *Evans, P. V.; Greer, A. L.:* Mat. Sci. Eng. 98 (1988), p. 357–61.
9) *Vogt, E.; Frommeyer, G.:* Proc. 1th Int. Conf. on Rapidly Solidified Materials, San Diego (1986), p. 291–97.
10) *Mühlbach, H.; Stephani, G.; Sellger, R.; Fiedler, H.:* Int. J. of Rapid Sol. 3 (1987), p. 83–99.
11) *Tenwick, M. J.; Davies, H. A.:* Proc. 5th Int. Conf. on Rapidly Quenched Metals, [eds.:] S. Steeb, H. Warlimont, Elsevier (1985), p. 67–70.